Published in *Catalysis Today 213 (2013) 219– 225*
doi:10.1016/j.cattod.2013.04.031

Effect of silicon content on the catalytic behavior of chabazite type silicoaluminophosphate in the transformation of methanol to short chain olefins

Teresa Álvaro-Muñoz, Carlos Márquez-Álvarez and Enrique Sastre*

Instituto de Catálisis y Petroleoquímica, ICP-CSIC.

C/ Marie Curie, 2, 28049. Madrid. Spain

Corresponding author: Dr. Enrique Sastre

E-mail: esastre@icp.csic.es

Abstract

AlPO-34 and SAPO-34 molecular sieves with different silicon content have been synthesized using a hydrothermal system in presence of tetraethylammonium hydroxide (TEAOH) and evaluated as catalysts for the transformation of methanol to short chain olefins. The results showed that SAPO-34 materials prepared with medium-high silicon concentration in the framework present quite similar silicon environment distributions

and, when it is so, the key factor to obtain materials with improved catalytic performance is the crystallite size.

Keywords:

AlPO-34; SAPO-34; silicon content; methanol-to-olefins.

1. Introduction

The global energy crisis has renewed the interest in developing technologies that allow diversifying the resources used to produce energy and fuels, as well as chemicals currently obtained from petroleum. Light olefins such as ethylene, propylene and butylenes are important intermediates for the petrochemical industry. They can be produced using several processes using mainly fossil, and therefore non-renewable, raw materials. However, it is necessary to seek alternative sources to satisfy the demand of these materials. In these sense, the production of light olefins from methanol is an attractive process because methanol can be obtained from a wide variety of materials. Methanol can be efficiently produced from syngas [1-3] obtained by natural gas reforming or carbon gasification, and it might even provide an environmentally carbon neutral alternative to fossil carbon sources [4], if produced by chemical recycling of carbon dioxide via hydrogenation [5] or from syngas obtained by biomass gasification [6].

The transformation of methanol to olefins (MTO process) can be effectively carried out by using small pore silicoaluminophosphates SAPO-34 (zeotype with chabazite structure) as catalyst [7, 8], obtaining exceptionally high selectivity to lower olefins. The influence of different synthesis parameters on the catalytic properties of these catalysts has been widely studied during the last few years. In this sense, the use of different structure directing agents (SDA) has a notable influence on the physicochemical properties and on the catalytic performance of SAPO-34 [9-15]. Moreover, extensive studies indicate that crystallite size and morphology affect catalyst properties and applications and, in this sense, it has been demonstrated that the catalytic performance of SAPO-34 can be strongly correlated with particle size due to the

diffusion limitations of the guest molecules in the micropores [14, 16-20]. Another parameter which could affect strongly the catalyst performance is the content and distribution of silicon in the SAPO framework, which determines the acid sites concentration and strength. In this sense, some authors have mentioned the effect of low Si content of SAPO-34 in the methanol transformation to olefins by reducing the deactivation rate and the propane production [21]. Other authors have estimated the stability and structure of silica species in SAPOs based on theoretical calculations [22] or investigated the kinetics of silicon substitution during SAPO-34 crystallization [23]. The acidity of the different species of silicon presented in SAPO-34 has been studied by different theoretical or experimental techniques, leading to differing conclusions. Several studies conclude that the acid strength is independent of the content of Si atoms or particle size [20, 24] or that the number of strong acid sites is independent of the silicon content [25]. However, other authors, based on FTIR, neutron diffraction and NMR experiments, have described the presence of three distinct Brönsted acid sites with different strength in SAPO-34 materials [26-31], confirming the previous asseveration of Sastre et al. [32] that the acid sites in the border of silicon islands are more acidic than those next to isolated Si species. In a recent contribution, we have demonstrated that samples of SAPO-34 obtained by adding a surfactant to a two-liquid phase synthesis gel show a different Si distribution than those synthesized in absence of surfactant [33]. SAPO-34 synthesized by using this method, present greater incorporation of silicon and a broader distribution of silicon environments in the network and therefore, a substantial increase in the material acidity. In conclusion, there are disagreements among the different authors about the role of the silicon content on the catalytic behaviour of SAPO-34 in the MTO process. In this sense, the objective of this paper is intending to clarify some contradictory results published up to now by different

authors on the role of the Si concentration in SAPO-34 materials on their catalytic behaviour in the MTO reaction. So, in this contribution we report the synthesis of SAPO-34 samples with different content of silicon in the framework and describe their physicochemical properties and catalytic behaviour in the MTO process trying to define clearly how the silicon content influences the performance of the SAPO-34 catalysts in the transformation of methanol to light olefins.

2. Experimental

2.1. Synthesis of SAPO-34 molecular sieves

AlPO-34 and SAPO-34 catalysts were synthesized by a hydrothermal method. Aluminium hydroxide hydrate (Sigma-Aldrich), 85% phosphoric acid (Riedel de Haën) and silica sol (30 wt. % suspension in water, Aldrich) were used as sources of the framework elements. Tetraethylammonium hydroxide (TEAOH, 35 wt. % solution in water, Aldrich) has been used as structure directing agent (SDA). Experimental conditions (temperature and crystallization times) have been adjusted in order to obtain pure phases of chabazite structure in all the cases. The gel composition was: $1Al_2O_3$: $1P_2O_5$: $xSiO_2$: yTEAOH: $40H_2O$ (x = 0-0.8; y = 1-1.5). The molar composition of the reaction mixtures and the synthesis conditions for the different AlPO-34 and SAPO-34 materials obtained are given in Table 1. In all the cases, syntheses were carried out at 423 K and crystallization time varied from 1 to 13 days. In a typical synthesis to get pure SAPO-34, the aluminium source –aluminium hydroxide – was added slowly to a dilute phosphoric acid solution, and the mixture was vigorously stirred for 2 h to obtain a uniform gel. Silica solution was then added dropwise to this mixture followed by

addition of the template (TEAOH). Finally, the mixture was stirred for about 4 h. The gel was then transferred into Teflon-lined stainless steel autoclaves with a capacity of 40 cc, which were heated statically at the required temperature under autogeneous pressure for the specified period of time. The resulting solids were collected by centrifugation, washed with water and ethanol and dried at room temperature overnight. The organic template and the water trapped within the micropores of the as-synthesized solids were removed by calcination at 823 K prior to catalyst testing. Complete removal of the organic molecule was assessed by thermogravimetric analysis.

2.2. Characterization

Powder X-ray diffraction (XRD) patterns of as-synthesized and calcined samples were recorded on a Philips X´PERT diffractometer using CuK_{α} radiation with a nickel filter. The textural data (pore volume and BET surface area) were determined by nitrogen adsorption at 77 K using a Micrometrics ASAP 2010 volumetric apparatus. Samples were degassed at 623 K under vacuum for at least 20 hours prior to measurement of the nitrogen adsorption/desorption isotherms. Due to the small size of pore windows of chabazite, prolonged equilibration times (of at least 20 s) were used in order to ensure that equilibrium was reached for every adsorptive dose. The crystallite size and morphology were analysed by scanning electron microscopy (SEM) using a JEOL JSM 6400 or a Philips XL30 microscopes, both operating at 20 kV.

The organic content of the samples was determined by elemental analysis with a Perkin-Elmer 2400 CHN analyser and by thermogravimetric analysis (TGA) using a Perkin-Elmer TGA7 instrument. TG analyses were carried out at a heating rate of 20 K/min

under air flow. Elemental analysis for Al, P and Si was performed for calcined samples by inductively coupled plasma optical emission spectrometry (ICP-OES, Perkin-Elmer 3300DV instrument) after sample dissolution by alkaline fusion.

^{29}Si CP/MAS NMR spectra were recorded at room temperature using a Bruker AV-400-WB spectrometer operating at 79.5 MHz, with a 4 mm probe spinning at 10 kHz. A $\pi/2$ pulse of 3 μs, contact time of 6 ms and recycle delay of 5 s were used. The chemical shifts were referenced to tetramethylsilane (TMS), taken as 0 ppm.

Ammonia temperature programmed desorption (NH_3-TPD) was performed using a ChemBET-3000 TPR/TPD, Quantachrome TPD equipment. Typically, 100 mg of sample pellets (20–40 mesh) were pre-treated at 823 K for 1 h in helium flow (25 mL/min) and subsequently cooled to the adsorption temperature (400 K). A gas mixture of 5.0 vol. % NH_3 in He was then allowed to flow over the sample for 4 h at a rate of 15 mL/min followed by helium flow for 30 min to remove weakly adsorbed NH_3. Finally, helium flow at a rate of 25 mL/min was passed over the sample with increasing temperature to 823 K at the rate of 10 K/min.

2.3. Catalyst testing

Methanol conversion to olefins was tested at 673 and 723 K in a continuous down flow packed bed reactor fully automated and controlled from a personal computer (PID Eng&Tech Microactivity Reference), operating at atmospheric pressure. Previous to the reaction, samples were pre-treated under nitrogen flow at 723 K for 1 hour. During the reaction, nitrogen was used as an inert diluent gas and co-fed with methanol into the reactor with a constant methanol/nitrogen ratio of 1/1 mol. Nitrogen feed was regulated

using a mass flow controller. Methanol was fed as liquid using a Gilson 307 HPLC pump, vaporized and mixed with the nitrogen stream in a pre-heater set at 473 K. Catalyst weight (1.0 g; 20-30 mesh pellets size) and methanol flow rate (0.100 ml/min) were adjusted in order to obtain a weight hourly space velocity (WHSV) of 1.2 h^{-1}. The reaction products were analysed on-line by gas chromatography using a Varian CP3800 gas chromatograph equipped with flame ionization (FID) and thermal conductivity (TCD) detectors, with a Petrocol DH5 0.2 capillary column and a Porapack Q 80-100 mesh packed column for separation of hydrocarbons and oxygenates, respectively.

3. Results and Discussion

According to the experimental procedure a series of samples of SAPO-34 and AlPO-34 has been synthesized. The experimental conditions and the gel compositions used for the different syntheses are presented in Table 1. In the case of SAPO materials, it was observed that when the silicon content in the synthesis gel was decreased to a SiO_2/Al_2O_3 ratio of 0.4 it was necessary to increase the concentration of the structure directing agent (TEAOH) to obtain materials with pure chabazite phase (sample S-34(4B) compared to sample S-34(4), which showed a mixture of CHA and AFI phases). Under the experimental conditions used in this work it has not been possible to synthesize pure SAPO-34 with higher silicon content than sample S-34(8) (with x = 0.8, Table 1). The X-ray powder diffraction patterns of the as-synthesized samples confirm the structure type SAPO-34 (CHA structure) in these materials (Figure 1). The peaks position and the intensities are identical to those reported for SAPO-34 [34]. As shown in Table 1, the syntheses carried out without silicon in the gel only rendered amorphous solids when the hydrothermal treatment was prolonged up to 5 days using the lowest

amount of SDA (y = 1). However, when the amount of TEAOH in the synthesis gel was increased up to y = 1.5, materials having pure chabazite phase were obtained for crystallization times from 1 up to 13 days [35]. XRD patterns of these samples are presented in Figure 2. It can be observed that the intensity of the XRD peaks of these samples increases with the crystallization time up to 7 days and then remain unchanged for longer times. For that reason, sample A-34-B7 has been selected to be compared with SAPO samples along this work. It is important to notice that AlPO samples present narrower diffraction peaks than the corresponding samples synthesized with silicon (Figure 1), probably pointing to a smaller crystallite size for the later samples.

The chemical and CHN elemental analyses of selected samples are detailed in Table 2. As it could be expected the amount of silicon incorporated to the solids increases linearly with the silicon concentration in the synthesis gel.

The organic content of the as-synthesized samples can be related with the incorporation of the SDA to the solids, which has been studied by thermogravimetric and elemental (CHN) analyses. Thermogravimetric analyses of these samples are plotted in Figure 3. Several weight loss steps can be observed in the TG profiles, depending on the sample. Samples S-34(6) and S-34(8) present a first weight loss, at temperatures of 323-343 K, which can be attributed to desorption of adsorbed water. The main weight loss, between 573 and 823 K, corresponds to the decomposition of the template (TEAOH) located inside the channels of the SAPO structure compensating the charge associated to the silicon atoms. Finally, the third weight loss at temperatures higher than 823 K has been associated with the further removal of organic residues occluded in the channels and cages of the SAPO-34 caused by combustion. Sample S-34(4B), in addition to these peaks, presents a notable weight loss at temperatures below 573 K which can be attributed to SDA physisorbed on the SAPO crystallites. It has been calculated that the

amount of TEA^+ cations required to fill up the void volume of SAPO-34 is around 1 molecule of template per chabazite cage, so the organic species in excess present in this sample should then be located probably on the external surface of the crystals. Finally, the AlPO sample A-34-B7 presents a different TG profile with the peaks corresponding to the desorption of water (temperature below 373 K), an important weight loss centred at 473 K attributed also to physisorbed SDA and an additional weight loss at 750-800 K which could be assigned to the removal of the organic residues by combustion.

The quantification of the different weight losses from the thermogravimetric analyses is presented in Table 3 and can be compared with the CHN elemental analyses (Table 2). It can be observed that values for the total amount of organic compounds in the solids determined from both techniques are in good agreement, considering the weight losses attributed to the SDA. The C/N ratios calculated from the elemental analyses are close to that corresponding to tetraethylammonium hydroxide (C/N = 8), indicating that the organic molecules occluded or adsorbed in the different samples should be mainly SDA molecules which are stable during all the synthesis.

The crystallite size and shape of the different samples has been determined by SEM (Figure 4). Both parameters seem to be influenced by the amount of silicon employed in the synthesis. The AlPO sample A-34-B7 presents a mixture of large rhombohedral crystallites of approximately 1 μm and very small nanocrystals with irregular shape, while SAPO samples present a more uniform morphology consisting in plate-like crystallites. The dimensions of crystallites are around 0.8 μm x 0.8 μm x 0.3 μm for sample S-34(4B). Crystallite size decreases when the amount of silicon in the material increases. In this sense, SEM micrographs of samples S-34(6) S-34(8) show that these

samples crystallize also with a plate-like morphology and crystallites of around 0.5 μm x 0.5 μm x 0.2 μm in size.

Textural properties of calcined materials were analysed by nitrogen adsorption–desorption at 77 K. All the SAPO-34 samples present type I isotherms (according to the IUPAC classification [36]), corresponding to microporous materials (Fig. I in Supplementary information). Data of surface area calculated from the isotherms are collected in Table 4. It can be observed that the samples have surface area in the range 420–650 m^2/g. The sample with larger crystallites (S-34(4B)) possesses the lower surface area and all the samples show very low non-microporous (external) surface, values characteristic of this type of materials.

^{29}Si CP/MAS NMR spectra of the SAPO samples are presented in Figure 5. It can be observed that the spectra obtained for the three samples are quite similar and consist of a broad envelope in the -80 to -120 ppm range, corresponding to several resonances due to different Si(nAl) environments (n=0-4), in which the Si atoms are tetrahedrally coordinated to oxygen atoms and surrounded by n Al and 4-n Si atoms in the second coordination sphere. Therefore, in these samples Si incorporation occurs not only by SM2 mechanism (substitution of one P atom by a Si atom in the AlPO framework) but also by simultaneous substitution of a pair of adjacent Al-P atoms (SM3 mechanism), thus giving rise to aluminosilicate domains (commonly referred to as Si islands) in the SAPO network which is in good agreement with observations published previously for SAPO-34 catalysts with similar silicon framework content [23, 31, 35]. The size and concentration of these Si islands will be different depending on the extension of SM3 to SM2 substitutions [37, 38] and this can be correlated with the strength of the acid sites generated at the border of the Si islands which is higher than that of the acid sites created by the isolated Si atoms [39]. Thus, a higher number of acid sites are generated

through the SM2 mechanism, while substitution via SM2 + SM3 yields less but stronger acid sites. In all the spectra shown in Figure 5, this broad band is centred at -100 ppm and only slight differences can be appreciated among the different samples. The broad spectra obtained for these samples, with maxima at around -100 ppm, indicate that there are both isolated Si atoms and very small silica domains, but no large silicon islands, in these catalysts.

The acidity of the calcined samples has been evaluated by NH_3-TPD (Figure 6). It can be observed that the AlPO material possess some acidity, although the total amount of adsorbed ammonia in that sample is significantly smaller than that obtained for the SAPO-34 samples. Besides, the TPD profile of the AlPO sample shows a maximum at around 525 K, indicating that these acid sites are relatively weak. This acidity could be related to weak Brönsted sites corresponding to terminal P-OH and/or Al-OH groups. However, it is well known that this technique does not allow distinguishing between Brönsted and Lewis acid sites. Therefore, it cannot be excluded that some Lewis acid centres able to adsorb ammonia at moderate temperature are present in the AlPO material, probably formed during the calcination treatment. SAPO-34 samples with different Si content show slightly different TPD profiles, although the total amount of ammonia adsorbed is similar for the three samples in spite of the different Si framework content. All three samples show a desorption peak with maximum at around 525 K, as in the case of the AlPO sample, that would correspond to weak acid sites, and an additional desorption peak at higher temperature (with maximum at around 625 K), which reveal the presence of stronger acid sites in these samples. The relative proportion of the high- and low-temperature desorption peaks changes with the total silicon content, indicating different distribution of acid strength. The sample with intermediate silicon content, i.e. S34(6), exhibits the highest proportion of stronger acid sites, while the sample with the higher silicon content, i.e. S34(8), possesses the lowest proportion of stronger acid sites, the weak acid sites being predominant.

Samples of AlPO-34 and SAPO-34 with different content of silicon in the framework have been tested in the transformation of methanol to short chain olefins at 673 and 723 K, under the experimental conditions described previously. Except the AlPO-34 catalyst, all the samples showed very high initial activity in the MTO reaction at both temperatures (Figure 7), and full conversion of oxygenates (both methanol and intermediate dimethyl ether) was obtained at short reaction time. In all the cases, the catalyst lifetime decreased when the temperature was increased from 673 to 723 K (Figure 7). The process is characterized by fast deactivation of the catalyst as a result of the formation of pore-blocking products in the course of the reaction, making the active centres of the catalyst less accessible for reactant molecules, and this mechanism is enhanced when the reaction temperature increases. All catalysts tested converted methanol with high selectivity to short chain (C_2-C_4) olefins, reaching values as high as 90-95 %, which only decayed slightly when the conversion levels started to decrease (Figure 8). For all the catalysts, the ethylene/propylene ratio increases with the reaction temperature (Supplementary Information, Figure II). $C_2^=/C_3^=$ ratios around 1 are obtained at 673 K while they increase up to 1.3-1.4 when the temperature rises at 723 K. This fact has been previously attributed to the secondary reactions of oligomerization and cracking which are favoured when the reaction temperature increases [40, 41].

It is important to remark that data in Figures 7 and 8 are referred to conversion of methanol into hydrocarbon products, that is, in products other than dimethyl ether. Therefore, conversion levels are determined as conversion of oxygenates (transformation of both methanol and dimethyl ether) and selectivity values indicate selectivity to the different hydrocarbons and are calculated excluding the intermediate product dimethyl ether. Thus, the low conversion values calculated for AlPO-34 are due

to the fact that this catalyst produces mainly dimethyl ether. Also, the decay of conversion levels of the SAPO-34 catalysts is due to the production of dimethyl ether that is observed once the catalysts deactivation starts. The lower activity of the AlPO-34 sample can be attributed both to its low concentration of acid sites and their weak acid strength (as shown by the NH_3-TPD analyses), associated with defects in the framework, since the absence of silicon in this catalyst precludes the presence of Brønsted acid centers like those characteristic of SAPO materials (Si-OH-Al). At both temperatures, as the reaction time increases, differences in the catalytic behaviour began to appear among the different samples. In the case of sample S-34(4B) conversion at 673 K goes down to less than 50% after 4 h of time on stream (TOS), while samples S-34(6) and S-34(8) maintain conversion levels above 90 % during 6 hours. As it is well known, the main problem of this kind of catalysts in the MTO process is the rapid deactivation attributed to the deposition of high molecular weight hydrocarbons on the pore entrances [7, 17, 42, 43], but it has been demonstrated that an adequate optimization of the synthesis parameters can lead to catalysts with improved lifetime [14, 15, 21, 44]. Among the different parameters that influence the stability of these catalysts, especially the crystallite size and the acid strength of the active centres have been considered the most important factors affecting the deactivation during the reaction. The NH_3-TPD results showed that the three SAPO-34 catalysts possess similar total concentration of acid sites, but different acid strength distribution. The TPD profiles indicate that the proportion of stronger acid sites increases in the order S34(8) < S34(4B) < S34(6). These results indicate that catalytic behaviour of this series of SAPO-34 samples is not determined mainly by acidity. The faster deactivation of sample S34(4B) should be attributed to the larger crystallite size of this catalyst. The smaller crystallites of samples S-34(6) and S-34(8) would facilitate the accessibility of

the reactant molecules to the acid sites and the diffusion of the reaction products and could justify their higher stability in the MTO process under the experimental conditions tested here. The fact that both samples showed comparable catalytic stability despite their different distribution of acid strength, also supports the hypothesis that crystallite size has a more important effect on catalytic behaviour than acidity.

From the results presented here it can be concluded that, under the experimental synthesis conditions used in this work, with relatively high concentration of silicon in the framework, the distribution of the silicon environments is quite similar for all SAPO catalysts, despite the different samples incorporate quite different amounts of silicon into their frameworks and, as different authors have proposed previously, it appears that this parameter has a minor effect in the catalytic performance of these materials [20, 24, 25]. Indeed, the catalysts with different silicon content showed similar total concentration of acid sites, although some differences in acid strength distribution were apparent, which nevertheless seemed not to have a significant effect on catalysts stability. On the contrary, the crystallite of the SAPO-34 catalysts has been shown as the key parameter to control the catalytic behaviour in order to obtain more stable materials with longer lifetime. The results demonstrate that samples synthesized with smaller crystallite rendered the best catalytic performance independent of the silicon content.

Conclusions

Different samples of SAPO-34 with different amounts of silicon in the framework have been synthesized by following a conventional hydrothermal method. The results showed that SAPO-34 materials prepared with medium-high silicon concentration in the

framework present quite similar silicon environment distributions and, when it is so, the key factor to obtain materials with improved catalytic performance is the crystallite size of the catalyst.

Acknowledgements

We are thankful for the financial support of the Spanish Ministry of Science and Innovation, projects MAT2009-13569 and MAT2012-31127. TAM acknowledges CSIC for a PhD grant.

Table 1. Synthesis of SAPO-34 and AlPO-34. Molar composition of gel:

$Al_2O_3 : P_2O_5 : x\ SiO_2 : y\ TEAOH : 40H_2O$

Sample	**x**	**y**	**Cryst. Time (d)**	**Product Phase**
S-34(8)	0.8	1	5	CHA
S-34(6)	0.6	1	5	CHA
S-34(4)	0.4	1	5	CHA+AFI
S-34(4B)	0.4	1.5	5	CHA
A-34-A1	0	1	1	Amorphous
A-34-A3	0	1	3	Amorphous
A-34-A5	0	1	5	Amorphous
A-34-B1	0	1.5	1	CHA
A-34-B3	0	1.5	3	CHA
A-34-B5	0	1.5	5	CHA
A-34-B7	0	1.5	7	CHA
A-34-B10	0	1.5	10	CHA
A-34-B13	0	1.5	13	CHA

Temperature of crystallization: 423 K

Table 2. Chemical and CHN elemental analyses of selected samples of SAPO-34 and AlPO-34

Sample	$Si/(Al+P)_{gel}$	$Si/(Al+P)_{solid}$	Organic content (wt%)				C/N	Mol
			C	H	N	Total	at. ratio	SDA/u.c.
A-34-B7	0	0	4.47	2.99	0.70	8.16	7.5	0.49
S-34(4B)	0.10	0.15	17.84	2.54	2.82	25.62	7.4	2.03
S-34(6)	0.15	0.20	9.77	2.60	1.55	13.92	7.4	1.00
S-34(8)	0.20	0.28	9.59	4.96	1.60	13.73	7.0	1.04

Table 3. Thermogravimetric analyses of selected samples of SAPO-34 and AlPO-34.

Sample	Weight loss (%)		
	T<573K	**573K<T<823K**	**T>823K**
A-34-B7	16.6	8.1	1.0
S-34(4B)	19.7	15.8	1.6
S-34(6)	3.1	14.2	1.8
S-34(8)	3.6	14.4	1.7

Table 4. Textural properties of selected calcined samples of SAPO-34.

Sample	Specific surface area (m^2/g)		
	S_{BET}	S_{micro}	S_{ext}
S-34(4B)	424	384	40
S-34(6)	652	608	44
S-34(8)	545	483	62

Figure Captions.

Figure 1. X-ray diffraction patterns of SAPO-34 samples synthesized with different amount of silicon in the synthesis gel. The asterisks indicate reflections showing the presence of and additional AFI phase.

Figure 2. X-ray diffraction patterns of AlPO-34 samples synthesized at different crystallization times.

Figure 3. Thermogravimetric analyses (solid lines) and derivatives (dotted lines) of AlPO-34 and SAPO-34 samples.

Figure 4. Scanning Electron Micrographs of AlPO-34 and SAPO-34 samples.

Figure 5. ^{29}Si CP/MAS NMR spectra of calcined SAPO-34 catalysts synthesized with different amount of silicon in the synthesis gel.

Figure 6. NH_3-TPD plots of calcined SAPO-34 catalysts synthesized with different amount of silicon in the synthesis gel.

Figure 7. Conversion of oxygenates (MeOH and DME) vs. reaction time obtained with the different catalysts. Test conditions: T= 673-723 K, WHSV = 1.2 h^{-1}, 1 g of catalyst.

Figure 8. Selectivity to short chain olefins (C2–C4) in function of the time on stream for the different samples in the MTO reaction. Test conditions: T= 673-723 K, WHSV = 1.2 h^{-1}, 1 g of catalyst.

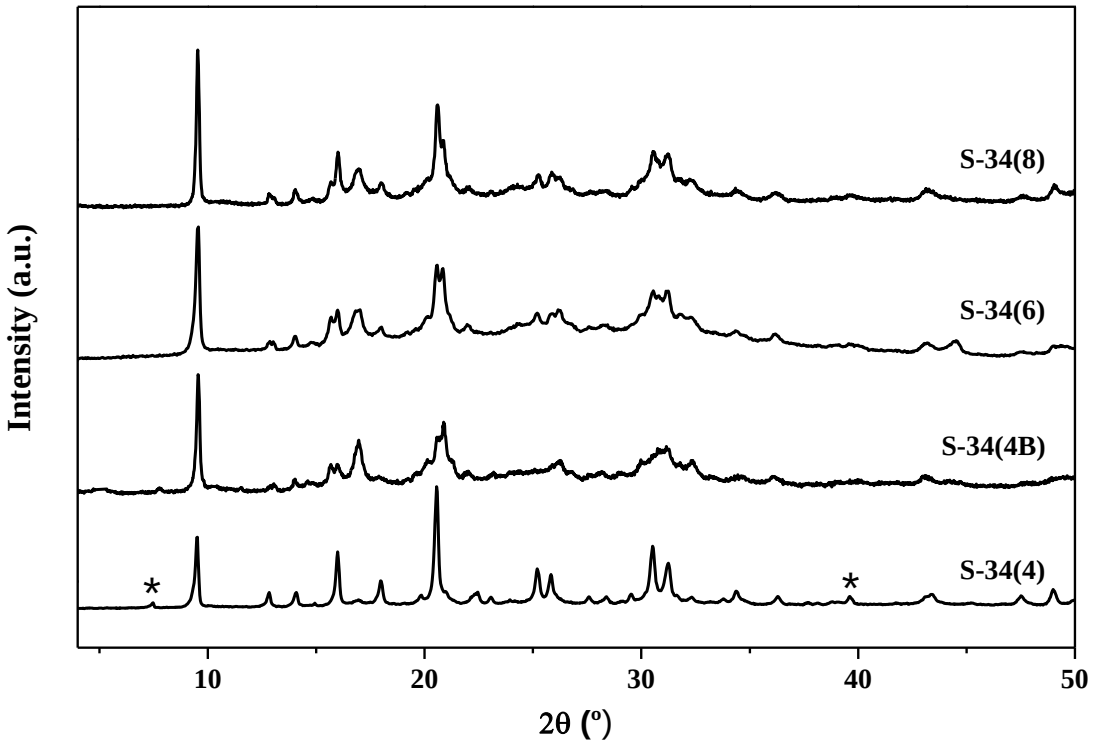

Figure 1

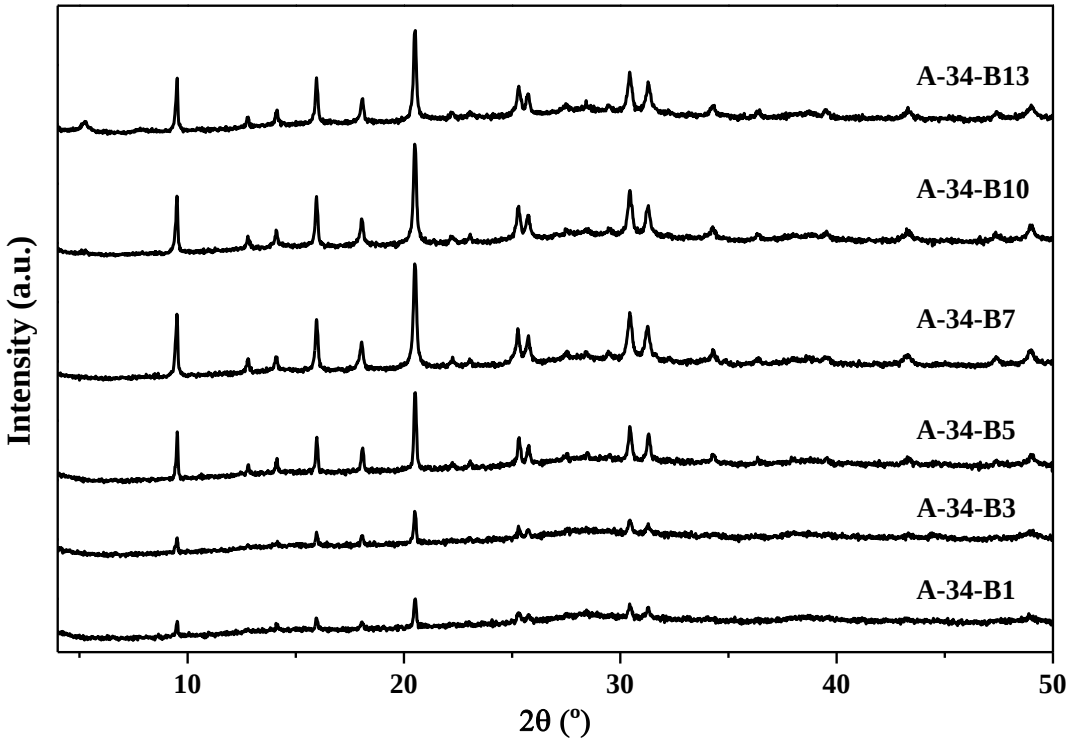
A-34-B13
A-34-B10
A-34-B7
A-34-B5
A-34-B3
A-34-B1
Intensity (a.u.)
10
20
30
40
50
2θ (º)

Figure 2

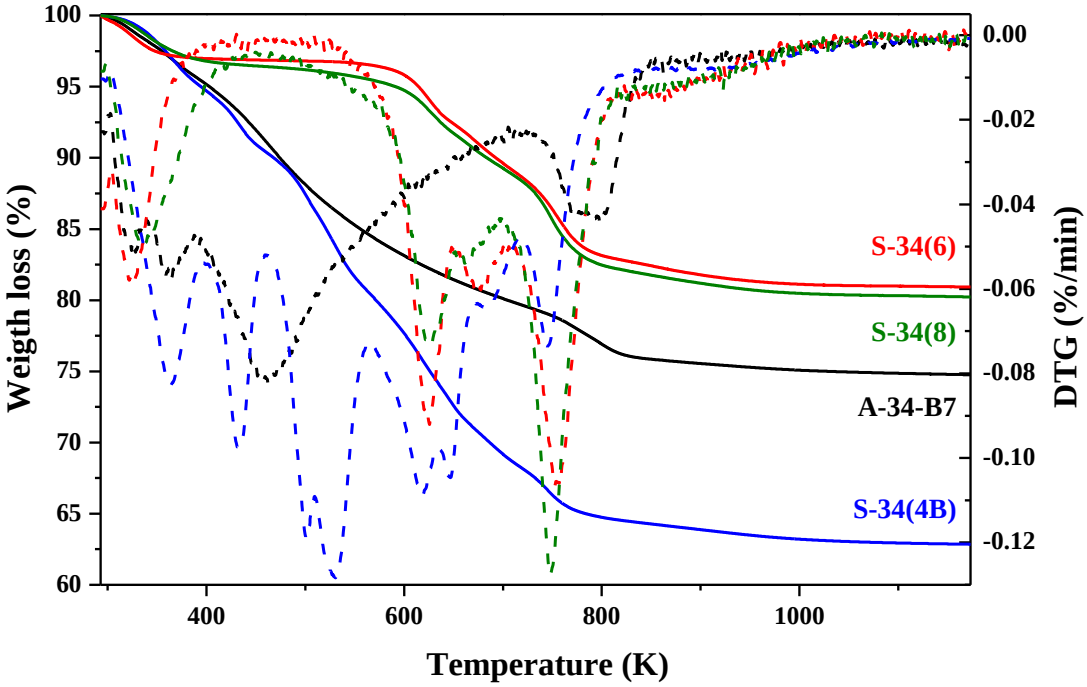
Weigth loss (%)
DTG (%/min)
Temperature (K)
S-34(6)
S-34(8)
A-34-B7
S-34(4B)
100
95
90
85
80
75
70
65
60
0.00
-0.02
-0.04
-0.06
-0.08
-0.10
-0.12
400
600
800
1000

Figure 3

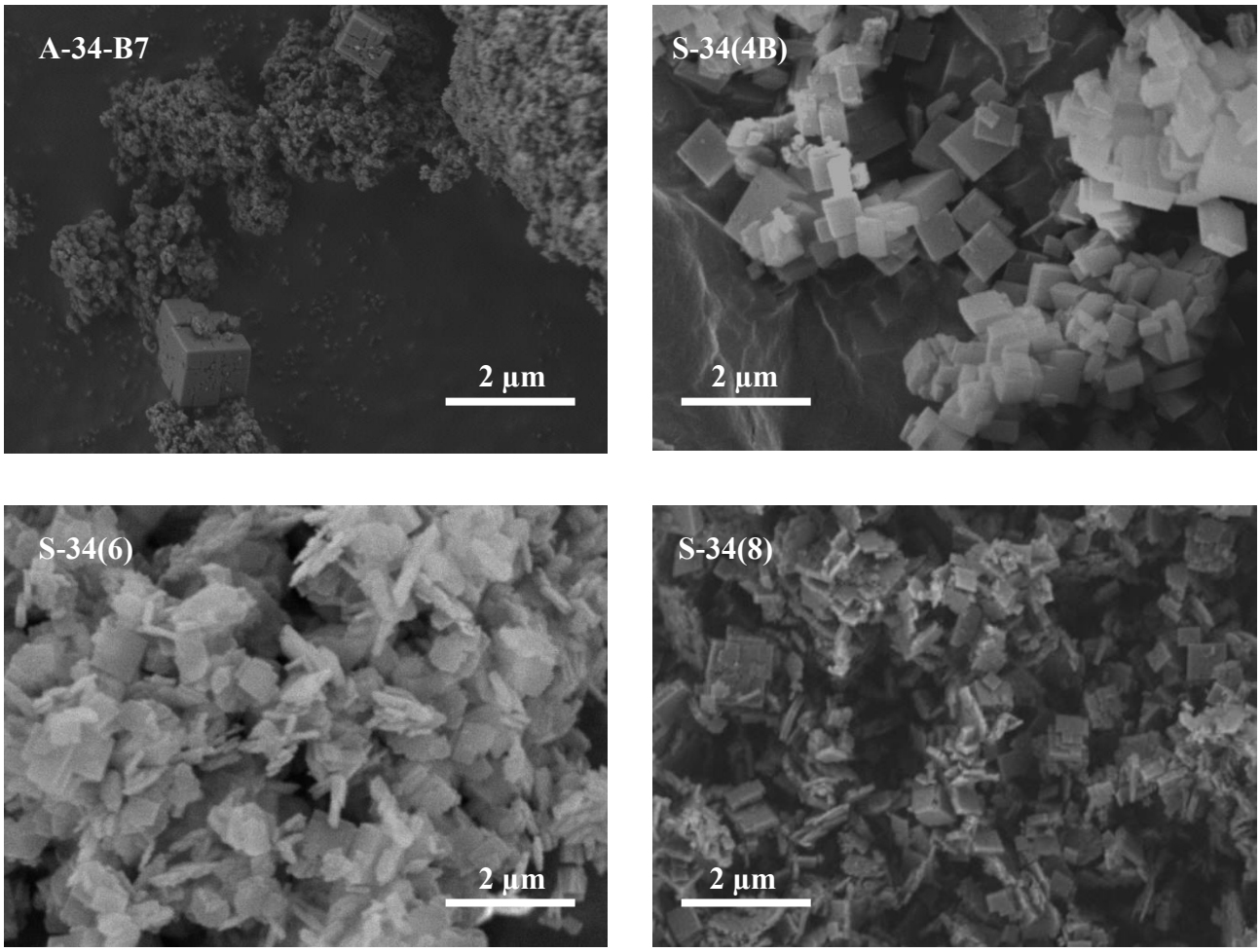

Figure 4

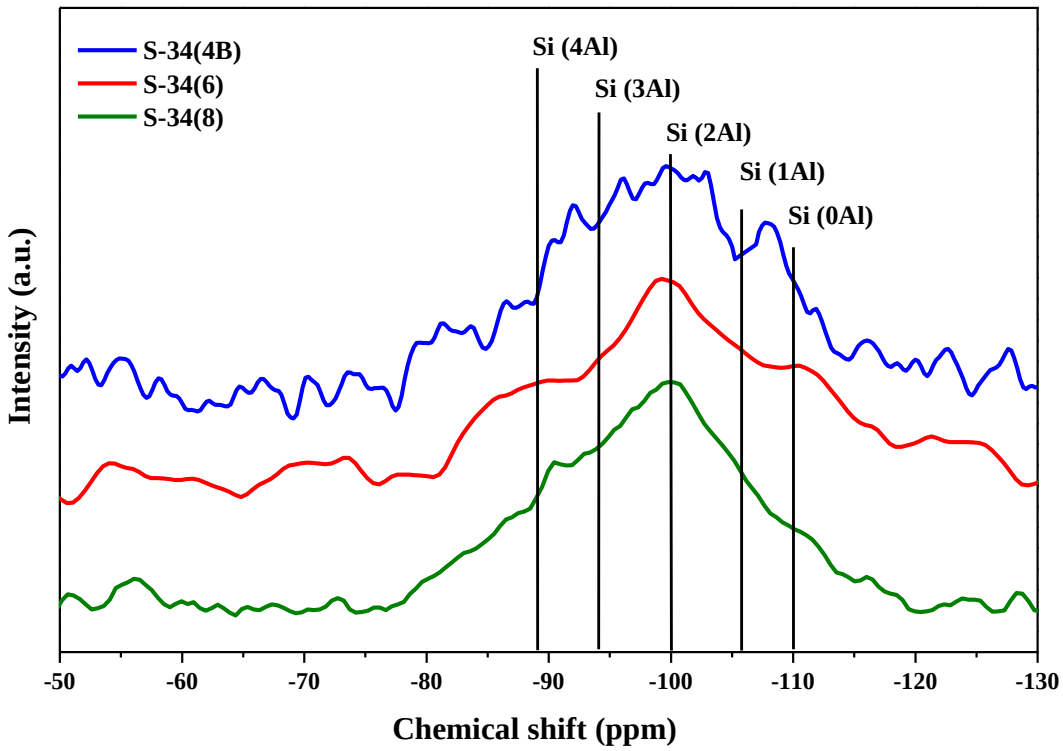
S-34(4B)
S-34(6)
S-34(8)
Si (4Al)
Si (3Al)
Si (2Al)
Si (1Al)
Si (0Al)
Intensity (a.u.)
-50
-60
-70
-80
-90
-100
-110
-120
-130
Chemical shift (ppm)

Figure 5

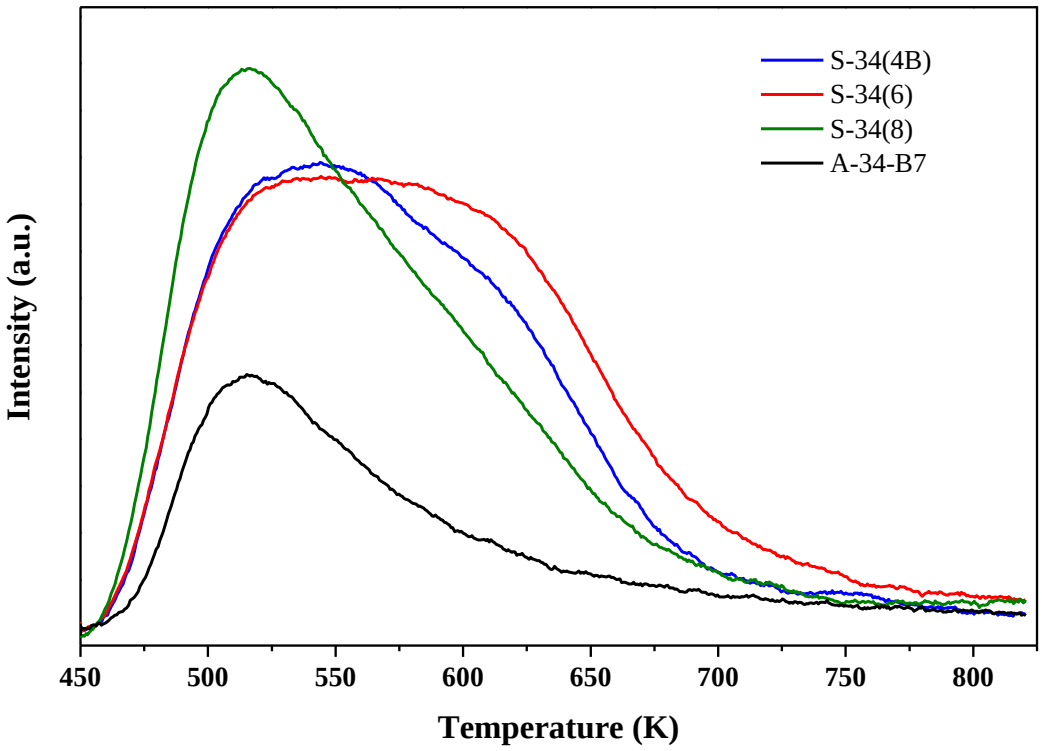
S-34(4B)
S-34(6)
S-34(8)
A-34-B7
Intensity (a.u.)
450
500
550
600
650
700
750
800
Temperature (K)

Figure 6

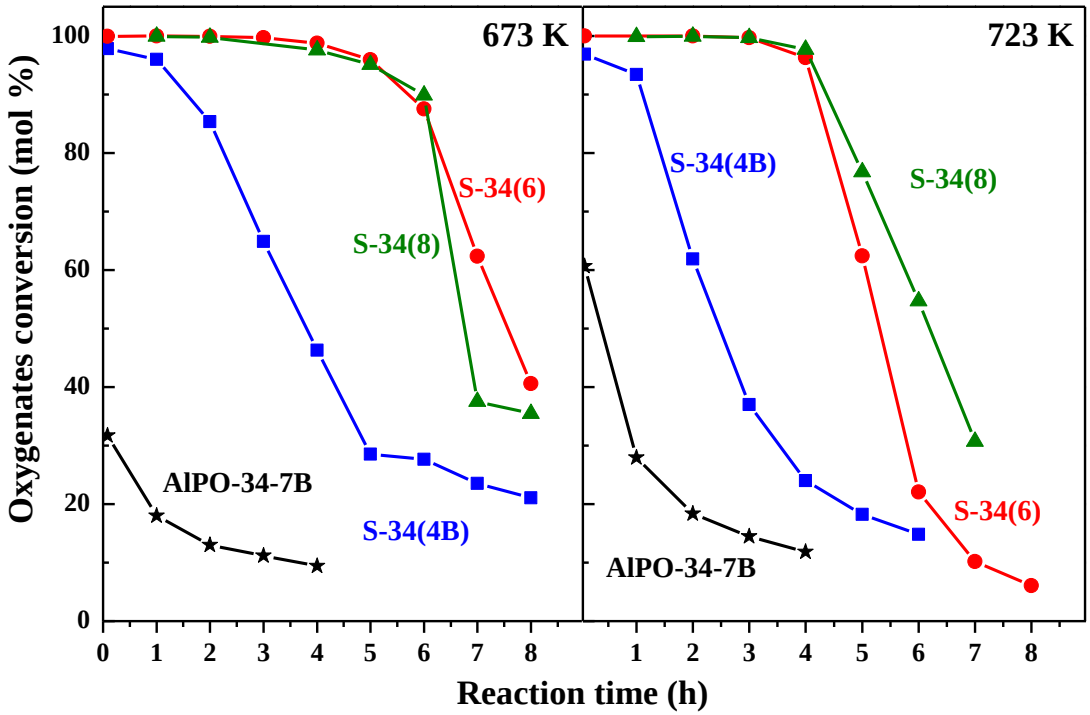
673 K
723 K
Oxygenates conversion (mol %)
Reaction time (h)
S-34(6)
S-34(8)
S-34(4B)
AlPO-34-7B
0
20
40
60
80
100
0
1
2
3
4
5
6
7
8

Figure 7

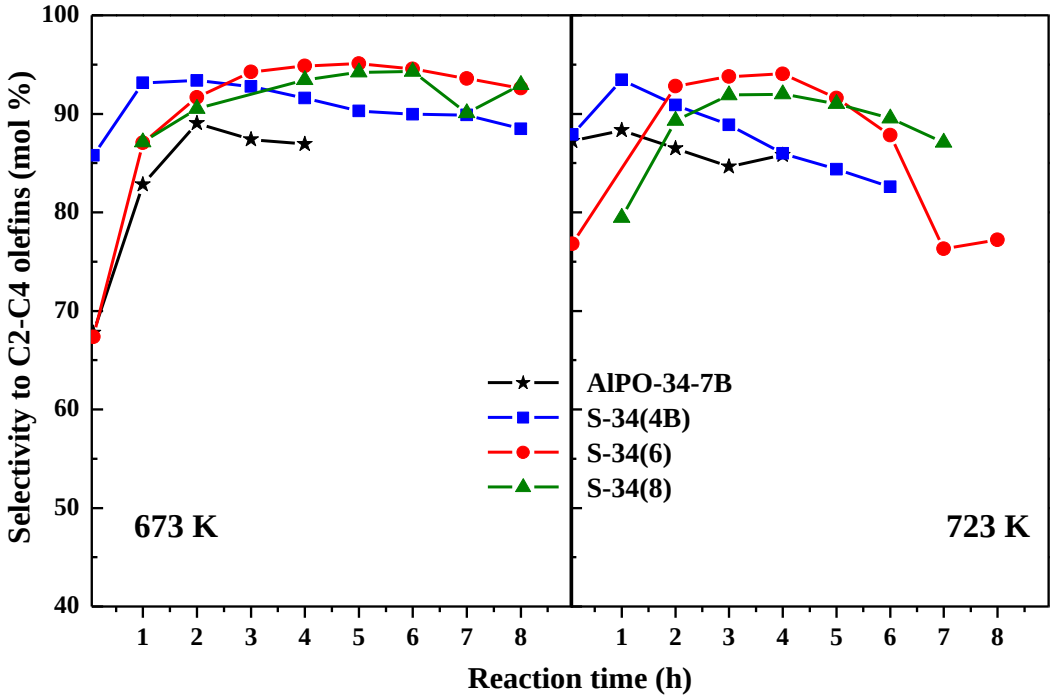
Selectivity to C2-C4 olefins (mol %)
100
90
80
70
60
50
40
1
2
3
4
5
6
7
8
Reaction time (h)
673 K
723 K
AlPO-34-7B
S-34(4B)
S-34(6)
S-34(8)

Figure 8

References

[1] A. Gotti, R. Prins, Journal of Catalysis 178 (1998) 511-519.
[2] I. Wender, Fuel Processing Technology 48 (1996) 189-297.
[3] C.V. Ovesen, B.S. Clausen, J. Schiotz, P. Stoltze, H. Topsoe, J.K. Norskov, Journal of Catalysis 168 (1997) 133-142.
[4] G.A. Olah, A. Goeppert, G.K.S. Prakash, Journal of Organic Chemistry 74 (2009) 487-498.
[5] C. Song, Catalysis Today 115 (2006) 2-32.
[6] C.N. Hamelinck, A.P.C. Faaji, Journal of Power Sources 111 (2002) 1-22.
[7] J. Liang, H. Li, S. Zhao, W. Guo, R. Wang, M. Ying, Applied Catalysis 64 (1990) 31-40.
[8] M. Stöcker, Microporous and Mesoporous Materials 29 (1999) 3-48.
[9] R. Vomscheld, M. Briend, M.J. Peltre, P.P. Man, D. Barthomeuf, Journal of Physical Chemistry 98 (1994) 9614-9618.
[10] E. Dumitriu, A. Azzouz, V. Hulea, D. Lutic, H. Kessler, Microporous Materials 10 (1997) 1-12.
[11] Y.-J. Lee, S.-C. Baek, K.-W. Jun, Applied Catalysis, A: General 329 (2007) 130-136.
[12] G. Liu, P. Tian, J. Li, D. Zhang, F. Zhou, Z. Liu, Microporous and Mesoporous Materials 111 (2008) 143-149.
[13] L. Ye, F. Cao, W. Ying, D. Fang, Q. Sun, Journal of Porous Materials 18 (2010) 225-232.
[14] T. Álvaro-Muñoz, C. Márquez-Álvarez, E. Sastre, Catalysis Today 179 (2012) 27-34.
[15] P. Wang, A. Lv, J. Hu, J.a. Xu, G. Lu, Microporous and Mesoporous Materials 152 (2012) 178-184.
[16] Y. Hirota, K. Murata, S. Tanaka, N. Nishiyama, Y. Egashira, K. Ueyama, Materials Chemistry and Physics 123 (2010) 507-509.
[17] D. Chen, K. Moljord, T. Fuglerud, A. Holmen, Microporous and Mesoporous Materials 29 (1999) 191-203.
[18] I.M. Dahl, R. Wandelbo, A. Andersen, D. Akporiaye, H. Mostad, T. Fuglerud, Microporous and Mesoporous Materials 29 (1999) 159-171.
[19] N. Nishiyama, M. Kawaguchi, Y. Hirota, D. Van Vu, Y. Egashira, K. Ueyama, Applied Catalysis, A: General 362 (2009) 193-199.
[20] Y. Iwase, K. Motokura, T.R. Koyama, A. Miyaji, T. Baba, Phys Chem Chem Phys 11 (2009) 9268-9277.
[21] S. Wilson, P. Barger, Microporous and Mesoporous Materials 29 (1999) 117-126.
[22] G. Sastre, D.W. Lewis, C.R.A. Catlow, Journal of Physical Chemistry 100 (1996) 6722-6730.
[23] J. Tan, Z. Liu, X. Bao, X. Liu, X. Han, C. He, R. Zhai, Microporous and Mesoporous Materials 53 (2002) 97-108.
[24] F.C. Sena, B.F. de Souza, N.C. de Almeida, J.S. Cardoso, L.D. Fernandes, Applied Catalysis, A: General 406 (2011) 59-62.
[25] A. Izadbakhsh, F. Farhadi, F. Khorasheh, S. Sahebdelfar, M. Asadi, Y.Z. Feng, Applied Catalysis, A: General 364 (2009) 48-56.
[26] W. Shen, X. Li, Y. Wei, P. Tian, F. Deng, X. Han, X. Bao, Microporous and Mesoporous Materials 158 (2012) 19-25.
[27] Y. Wei, D. Zhang, Z. Liu, B. Su, Journal of Catalysis 238 (2006) 46-57.
[28] S. Bordiga, L. Regli, C. Lamberti, A. Zeccina, M. Bjorgen, K.P. Lillerud, Journal of Physical Chemistry B 109 (2005) 7724-7732.
[29] G.A.V. Martins, G. Berlier, S. Coluccia, P. H.O., G.B. Superti, G. Gatti, L. Marchese, Journal of Physical Chemistry C 111 (2007) 330-339.
[30] L. Smith, A.K. Cheetham, L. Marechese, J.M. Thomas, P.A. Wright, J. Chen, E. Gianotti, Catalysis Letters 41 (1996) 13-16.

[31] L. Xu, A. Du, Y. Wei, Y. Wang, Z. Yu, Y. He, X. Zhang, Z. Liu, Microporous and Mesoporous Materials 115 (2008) 332-337.
[32] G. Sastre, D.W. Lewis, Journal of the Chemical Society, Faraday Transactions 94 (1998) 3049-3058.
[33] T. Álvaro-Muñoz, C. Márquez-Álvarez, E. Sastre, Catalysis Today Submitted.
[34] B.M. Lok, C.A. Messina, R.L. Patton, R.T. Gajek, T.R. Cannan, E.M. Flanigen, Crystalline silicoaluminophosphates US Patent 4 440 871, 1984.
[35] A. Izadbakhsh, F. Farhadi, F. Khorasheh, S. Sahebdelfar, M. Asadi, Z.F. Yan, Microporous and Mesoporous Materials 126 (2009) 1-7.
[36] K.S.W. Sing, D.H. Everett, R.A.W. Haul, L. Moscou, R.A. Pierotti, J. Rouquerol, T. Siemieniewska, Pure and Applied Chemistry 57 (1985) 603-619.
[37] A.M. Prakash, S. Unnikrishnan, K.V. Rao, Applied Catalysis, A: General 110 (1994) 1-10.
[38] J.A. Martens, C. Janssens, P.J. Grobet, H.K. Beyer, P.A. Jacobs, Studies in Surface Science and Catalysis 49 (1989) 215-225.
[39] S. del Val, T. Blasco, E. Sastre, J. Pérez-Pariente, Journal of the Chemical Society, Chemical Communications (1995) 731-732.
[40] M. Popova, C. Minchev, V. Kanazirev, Applied Catalysis, A: General 169 (1998) 227-235.
[41] X. Wu, M.G. Abraha, R.G. Anthony, Applied Catalysis, A: General 260 (2004) 63-69.
[42] A. Gronvold, K. Moljord, T. Dypvik, A. Holmen, Studies in Surface Science and Catalysis 81 (1994) 399-404.
[43] D. Chen, H.P. Rebo, A. Gronvold, K. Moljord, A. Holmen, Microporous and Mesoporous Materials 35–36 (2000) 121–135.
[44] H.-G. Jang, H.-K. Min, J.K. Lee, S.B. Hong, G. Seo, Applied Catalysis, A: General 437-438 (2012) 120-130.